SWAN: A surface-towed modular controlled-source electromagnetic system for mapping submarine groundwater discharge and offshore groundwater resources

Anna Eliana Pastoressa[1], Amir Haroon[2,3], Mark E. Everett[4], Lea Rohde[2], Thies Bartels[2], Martin Wollatz-Vogt[2], Zahra Faghih[2], Gesa Katharina Franz[2], and Aaron Micallef[1,5]

https://doi.org/10.1190/tle42090590.1

Abstract

Offshore freshened groundwater (OFG) and submarine groundwater discharge (SGD) are important components of coastal hydrologic systems. A lack of understanding of offshore groundwater systems and their interactions with onshore systems along the majority of global coastlines still exists due to a general paucity of field data. Recently, controlled-source electromagnetic (CSEM) techniques have emerged as a promising noninvasive method for identifying and characterizing OFG and SGD. Unfortunately, only a few systems are available in academic and research institutions worldwide, and applications are limited to specific regions. These systems are often limited by relatively high deployment costs, slow data acquisition rates, logistical complexity, and lack of modification options. A relatively inexpensive and user-friendly CSEM system is needed to overcome these limitations. We present the initial theoretical and practical developments of SWAN — a low-cost, modular, surface-towed hybrid time-frequency domain CSEM system capable of detecting OFG and SGD to water depths of 100 m. A field test of the system was carried out in the central Adriatic Sea at water depths between several tens to approximately 160 m to illustrate its capabilities. Through its ability to facilitate continuous measurements in both the time and frequency domain, the system has demonstrated its effectiveness in acquiring high-quality data while operating at towing speeds ranging from 2.5 to 3 kn. The resulting data coverage enables the system to detect variations in subsurface resistivity to depths of approximately 150–200 m below seafloor. With its modular, user-friendly design, SWAN provides an accessible, cost-efficient means to investigate the hydrogeology of shallow offshore environments.

Introduction

Groundwater is an essential natural resource that plays a crucial role in sustaining ecosystems and supporting human needs. In coastal areas, where a disproportionately high population density exists, groundwater is of particular importance. Here, the vulnerability of potable groundwater resources is particularly high due in large part to groundwater emplacement during past glacial maxima and the interaction of terrestrial groundwater with its offshore counterpart.

Submarine groundwater discharge (SGD) and offshore freshened groundwater (OFG) resources are key components of coastal hydrogeology worldwide (Figure 1). However, their inaccessibility fosters our limited understanding of their spatial distribution and dynamics. Burnett et al. (2003) and Taniguchi et al. (2019) define SGD as the flow of water from the seabed to the coastal ocean, regardless of fluid composition or driving force. OFG, on the other hand, refers to water that is stored in pores of sediments and fractures in the subseafloor with total concentration of dissolved solids below that of seawater (Micallef et al., 2021).

Traditionally, the investigation of SGD and OFG has relied on drilling, borehole logging, core analysis, and water sampling at discharge sites, all of which are point-scale measurements with limited spatial coverage. In recent years, marine controlled-source electromagnetic (CSEM) techniques have emerged as a promising noninvasive geophysical method with contiguous wide-area coverage to help delineate the regional extent of freshened groundwater away from point-scale "ground-truthing" sites (e.g., Evans and Key, 2016; Haroon et al., 2018, 2021; Levi et al., 2018; Gustafson et al., 2019; Attias et al., 2020, 2021; Lippert and Tezkan 2020; Micallef et al., 2020; King et al., 2022).

Marine CSEM methods utilize electromagnetic signals generated by an artificial and controllable source to explore the geologic subsurface. A time-variant electric current in the transmitter induces an electromagnetic field in the seafloor that propagates

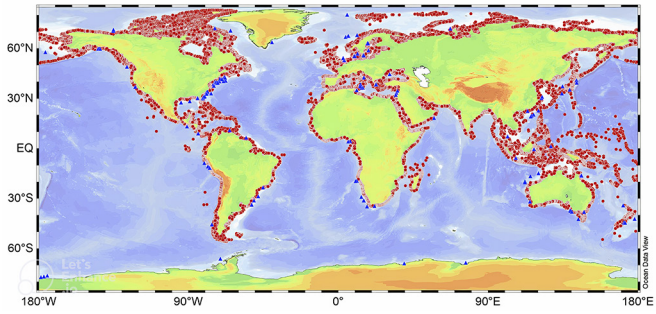

Figure 1. Global distribution of reported fresh SGD (red) and OFG (blue) sites. The locations are adapted from Luijendijk et al. (2020) and Micallef et al. (2020). The image is from Arévalo-Martinez et al. (2023).

[1]University of Malta, Department of Geosciences, Marine Geology and Seafloor Surveying, Msida, Malta. E-mail: eliana.pastoressa@um.edu.mt; aaron.micallef@um.edu.mt.
[2]GEOMAR Helmholtz Centre for Ocean Research Kiel, Kiel, Germany. E-mail: aharoon@geomar.de; lrohde@geomar.de; tbartels@geomar.de; mwollatz-vogt@geomar.de; zfaghih@geomar.de; gfranz@geomar.de.
[3]University of Hawai´i at Mānoa, Hawai´i Institute of Geophysics and Planetology, School of Ocean and Earth Science and Technology, Honolulu, Hawaii, USA. E-mail: aharoon@hawaii.edu.
[4]Texas A&M University, Department of Geology and Geophysics, College Station, Texas, USA. E-mail: everett@geo.tamu.edu
[5]Monterey Bay Aquarium Research Institute, Moss Landing, California, USA.

through different geologic formations and is modified by the electric resistivity of the different strata encountered. This perturbed field is measured by an array of receivers located at different distances from the transmitting source, allowing the electromagnetic signals to map the subsurface at various depths. Because fresh and saline pore fluids exhibit distinct electrical resistivity values, CSEM methods present an effective means of determining fluid properties in the subseafloor. While CSEM techniques show great promise in imaging freshened pore fluid beneath the seafloor, they have not yet been employed widely.

Commercially available electromagnetic survey systems, for example, are not well-suited for shallow marine environments. Designed primarily for oil and gas exploration, these systems are suboptimal for investigating the upper few hundred meters of the seafloor in shallow-water settings. They are cumbersome to deploy, transmit high currents that require trained personnel for safe operation, lack sensitivity to detect shallow seabed structures, and provide limited data resolution for characterizing the target of interest (OFG or SGD). Use of the available commercial systems for near-coastal groundwater research requires costly adaptations.

Only a few research groups have successfully developed and deployed in-house electromagnetic survey systems capable of operating in these environments. These groups include the Federal Institute for Geosciences and Natural Resources, GEOMAR Helmholtz Centre for Ocean Research (e.g., Haroon et al., 2021), and the University of Cologne (e.g., Schwalenberg and Engels, 2011; Haroon et al., 2018) in Germany; the National Oceanography Centre (Attias et al., 2016) in the United Kingdom; Ocean University of China (e.g., Wang et al., 2021) and China University of Geosciences (Jing et al., 2016) in China; and Scripps Institution of Oceanography, Woods Hole Oceanographic Institution, and Columbia University in the United States (e.g., Sherman et al., 2017; Gustafson et al., 2019; King et al. 2022). Among these approaches, some involve pulling a system along the seabed and stopping at predetermined stations (Yuan and Edwards, 2000; Gehrmann et al., 2015; Micallef et al., 2020), while others continuously tow a system through the water column (e.g., Constable et al., 2016; Sherman et al., 2017; Gustafson et al., 2019). These academic systems, although suitable for shallow waters, are characterized by one or multiple drawbacks such as relatively high deployment cost, slow data acquisition, logistical complexity, or limited customization options. Moreover, it is important to note that not all the academic systems have the capability to effectively map SGD in the water column because data may not be acquired continuously along profile.

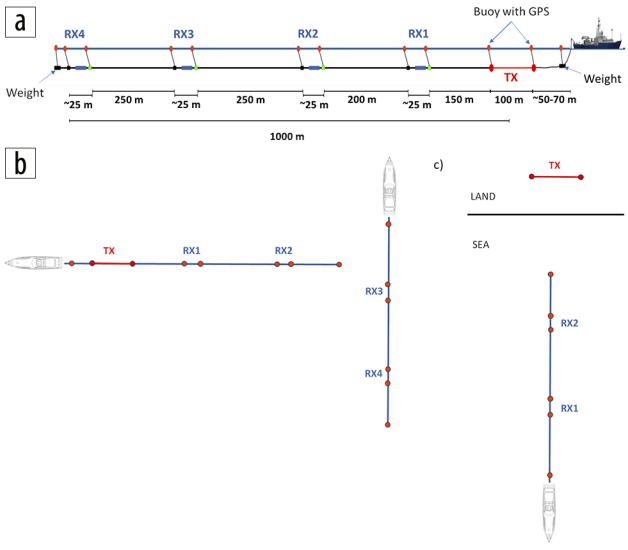

Figure 2. SWAN surface-towed CSEM system set up for (a) in-line measurements, where horizontal electric dipole transmitter (TX) and receivers (RX) are towed in-line behind a vessel; (b) 3D measurements, where one vessel tows a shortened array of in-line horizontal electric dipole transmitter and two receivers and a second or third vessel, moving independently of the first, tows only receivers; (c) amphibious measurements, where the horizontal electric dipole is placed onshore and receivers are towed offshore by one or more vessels.

The CSEM system presented in this paper addresses some of the aforementioned issues, specifically the development of a cost-effective method for acquiring electromagnetic data in both the time and frequency domains, thereby mitigating the slow acquisition speed of time-domain CSEM systems. Moreover, the system is reconfigurable, allowing for different receiver types, orientation, and location to target various depths at selected resolutions (Figure 2). The system can facilitate investigations in both the water column and in the shallow subseafloor in water depths less than 100 m. Here, we provide an account of the development process of the SWAN system, including system design, functionality, and preliminary results from a first field trial in the central Adriatic Sea.

A key aspect of our methodology entailed an extensive study to determine the optimal offsets and frequencies for investigating freshened pore fluid in the subseafloor (OFG) and SGD. To accomplish this, we examined electromagnetic field distributions using 1D synthetic modeling. Through this analysis, we gained insights into the system's sensitivity to different characteristics of the aquifer layers, enabling us to identify suitable combinations of offsets and frequencies. By refining the system parameters based on these findings, we enhanced its performance in detecting and characterizing OFG.

To evaluate the system's functionality under realistic conditions, we conducted field tests in the central Adriatic Sea, offshore Italy. This area was selected based on pre-existing geologic and seismic data that indicate the possible presence of freshened groundwater (e.g., Amorosi et al., 2016; Pellegrini et al., 2018). The field tests were used to validate the system's effectiveness in identifying and assessing the presence of OFG and to evaluate its applicability and performance.

Throughout the development process, we placed emphasis on efficiency and cost-effectiveness. We optimized the design parameters of the SWAN system by leveraging existing commercial instrumentation and conducting rigorous investigations. By presenting our findings, we aim to contribute to the advancement of CSEM technology for imaging freshened pore fluid in marine environments and encourage others to use the presented information as a blueprint for developing their own CSEM technologies.

It is worth acknowledging that the SWAN system bears similarities to the towed-streamer system described by Engelmark et al. (2014). SWAN represents a scaled-down version of the towed-streamer system, with modifications tailored specifically for investigating shallow-water structures such as SGD and OFG. While existing commercial systems generally are not designed

DOI:10.1190/tle42090590.1

with shallow-structure mapping in mind, the SWAN system fills this gap by providing a cost-effective solution for acquiring high-density electromagnetic data in near-coastal areas. By explicitly acknowledging the technology described by Engelmark et al. (2014), we aim to highlight the parallels between the SWAN system and existing approaches while emphasizing the unique features and focus of the SWAN system.

Methodology

The SWAN system follows the surface-towed concept, which has demonstrated high efficiency and effectiveness for near-coastal investigations. The surface-towed configuration generally allows for rapid data acquisition in shallow water while avoiding the environmental destruction caused by seafloor towing. Moreover, it overcomes the limitations of slower survey speeds associated with stationary seafloor nodes used for CSEM data collection. The SWAN system is designed to acquire data in both time and frequency domain to facilitate a variety of applications near the shoreline (Figure 2).

Instrument design. The SWAN CSEM system (Figure 2) was developed utilizing existing geophysical components available on the market, namely the ZT-30 transmitter from Zonge International and self-potential data loggers from Magson GmbH. The system has been configured as a surface-towed, dipole-dipole system designed for electrical exploration of the seafloor. It consists of a 100 m long horizontal electrical transmitter dipole and an array of up to four 25 m long autonomous receiver units, each carrying a 10 m long horizontal electrical dipole. In the towed configuration, these receiver units are connected in-line along a rope at various offsets and they function autonomously, as illustrated in Figure 2. The receiver units and control unit are powered by battery and have a lifespan of more than 72 hours. Each unit includes its own data logger and front-end electronics housed in a titanium pressure cylinder, although other materials such as aluminum or acrylic plastic may be used to reduce costs. Data can be sampled at frequencies up to 10 kHz. GPS is used to maintain time synchronization, which is further supported by a chip-scale atomic clock. The receiving dipoles are equipped with a pair of Ag/AgCl electrodes from Silvion affixed to the pressure cylinders of the receiver units. The source signal is generated by a current transmitter onboard the research vessel, capable of producing up to 30 A current for arbitrary step functions. A control unit records the transmitted currents and voltages. The transmitter and receiver are synchronized using GPS, and positioning is continuously determined using GPS tracking on multiple buoys located at each transmitter electrode, above each receiver, and at the tail of the streamer. To mitigate potential damage from ship traffic, the streamer depth can be adjusted prior to deployment between 1 and 10 m below sea surface. The focus of the development shifted toward the design of a carrier streamer with sufficient strain to be deployed from small- to medium-scale research vessels, fulfilling the requirements of a high-quality instrument at comparably low cost. It is important to note that alternative transmitter and receiver embodiments exist on the market and could be deployed on the SWAN carrier system.

The different segments that comprise the system, from receivers to placement buoys, are connected to the towrope through soft shackles applied at each joint, making the system modular with only a few metallic components. The design of a modular system in which the different elements are mounted through simple click-in connections makes it possible to adapt the system to different target depths, facilitating various types of measurements. As shown in Figure 2a, the arrangement of different modules on different carrier configurations enables the eventual acquisition of additional components of the electromagnetic field, which facilitates efficient 3D surveying (see Figure 2b). The data loggers from Magson GmbH are equipped with three channels for measurement of all electrical field components. Deploying the transmitter onshore allows for amphibious CSEM measurements crossing the shoreline (see Figure 2c) to capture the connectivity of terrestrial groundwater layers with potential SGD and OFG sites.

Sensitivity to target. Before conducting each CSEM survey, it is crucial to address key practical survey design questions to ensure the effectiveness of the investigation. These questions include determining the optimal distance between a transmitter and receivers, assessing anticipated signal levels, and identifying the most suitable source frequencies. These parameters can be influenced by various factors, including the thickness and resistivity of the subsurface layers. For instance, the choice of the distance between the transmitter and receivers depends on the depth of investigation required to detect the target features. A deeper target might necessitate larger transmitter-receiver offsets to penetrate the subsurface effectively, while a shallower target may require smaller offsets for higher resolution (e.g., Chave et al., 2017). The selection of the frequency source is also vital because different frequencies offer varying depths of penetration and sensitivity to different subsurface resistivity structures. Higher frequencies provide higher resolution but have reduced penetration depths, while lower frequencies can reach deeper targets but might sacrifice resolution (Spies, 1989).

Furthermore, the thickness and resistivity of the subsurface layers play a significant role in determining the amplitude and phase of the CSEM response. Understanding how these parameters influence the CSEM data can help in interpreting the results and distinguishing anomalies related to OFG or other subsurface features. To determine these parameters (optimal distance between a transmitter and receivers and optimal source frequencies), sensitivity studies using typical OFG models were conducted. To achieve this goal, tests employing 1D synthetic modeling were conducted using code developed by Everett and Chave (2019). The 1D synthetic models are built based on the outcomes of Micallef et al. (2021), who analyzed a database describing 305 OFG occurrences in different continental margins. The study found that most OFG bodies are located within 55 km of the coast, both in carbonate and siliciclastic systems, down to a water depth of 100 m. They usually occur in the shallowest parts of the subseafloor (first hundred meters).

A canonical plane-layered 1D model with water depth of 50 m and seawater conductivity of 5.0 S/m (conductivity of Mediterranean seawater) was developed. The first overburden sediment layer had a thickness of 30 m and a conductivity of 0.7 S/m, and the subsequent aquifer layer was 50 m thick with low conductivity (0.09 S/m). The in-line response of the electric

field generated by a horizontal electric dipole towed on the subsurface was computed as shown in the results section.

Field survey. The SWAN system was field tested on board the vessel G. Dallaporta in the central Adriatic Sea in May 2023, specifically in the coastal zone between the Tronto River in Ancona, Marche region, and the Fortore River in Foggia, Apulia region.

The western Adriatic Basin, formed during the early stages of the Apennine orogeny, is a Plio-Quaternary foredeep basin that has shifted eastward due to Apennine subduction (Cattaneo and Trincardi, 1999) and is characterized by a mud-dominated, transgressive sedimentary succession influenced by eustatic sea-level variations (Maselli et al., 2011). The presence of coarser layers at 20–90 m depths suggests the presence of fluvial channels from the Alpine and Apennine mountain chains (Asioli et al., 2001), which could potentially serve as freshwater reservoirs.

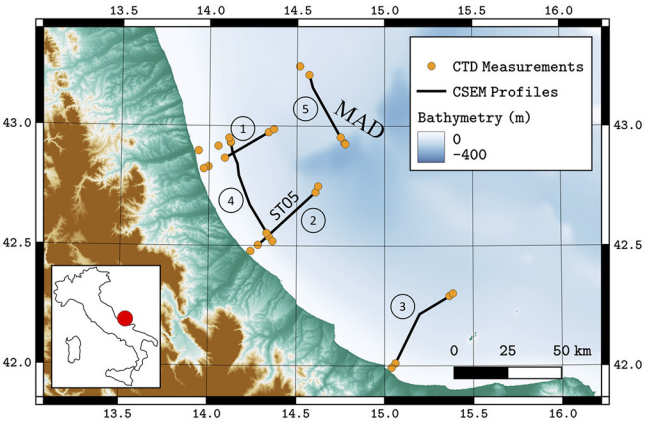

Figure 3. Digital elevation map of central Adriatic western coast (from Tarquini et al., 2023). Black solid lines are five profiles of CSEM measurements, while yellow dots denote points of CTD measurements or grab sampling. Locations of CTD measurements are courtesy of Claudio Pellegrini, Alessandra Mercorella (CNR Italy), and Bruno Campo (University of Bologna). ST05 indicates seismic profile interpreted from Maselli et al. (2011) and reported in Figure 8.

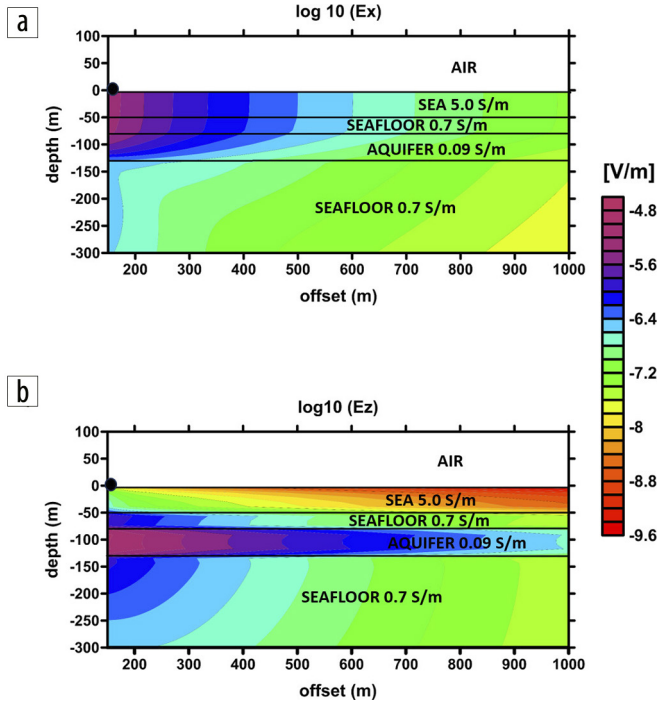

Figure 4. In-line (a) horizontal electric field and (b) vertical electric field responses for a layered aquifer model. The color scale depicts the amplitude of the corresponding electric field components. The black dot is the transmitter source located at offset = 0 m, and the frequency source was set to 1 Hz.

We aimed to investigate the uppermost 100 m below the seafloor along transects in the central Adriatic Sea using the SWAN system. To efficiently acquire high-quality data, the system was employed in the in-line configuration, utilizing two receivers placed approximately 260 and 520 m from the transmitter at a depth of 7 m below sea surface. Each deployment and recovery of the system, which involved winding and unwinding it from drums, required approximately 40 minutes.

Data acquisition was performed continuously along five acquisition profiles (see Figure 3) covering a total length of approximately 176 km. These profiles were completed over five days, with approximately 9 hours of operation per day at an average acquisition speed of approximately 2.5 kn.

A square-wave current signal of period 4 s, 25 A current, and 50% duty cycle was transmitted and injected into the subsurface via a 100 m horizontal electrical dipole along profiles 1 and 2. For profiles 3, 4, and 5, an input signal period of 2 s was used because preliminary data processing showed that 1 s transients are not necessary to reach direct current at the defined source-receiver offsets. By reducing the period to 2 s, more signals are measured, increasing the amount of available data for stacking to further improve the signal-to-noise ratio. A 50% duty cycle signal (time-domain acquisition) ultimately was chosen as the preferred acquisition waveform for this survey because uncertainties remained regarding heat development in the ZT-30 transmitter. The 50% duty cycle is conservative in this respect as signal is only transmitted 50% of the time, given that a 100% duty cycle transmission for multiple hours turned out to be feasible in a cooled laboratory environment. Conductivity-temperature-depth (CTD) sensor data were collected at the start and end of each measurement profile to complement the acquired CSEM data and constrain the resistivity profile of the water column for the subsequent inversion process. Although the system is technically able to function continuously over multiple days of acquisition, the collected data were downloaded and reviewed daily.

To demonstrate that the measured data are interpretable with plausible resistivity models, an exemplary excerpt of the acquired time series was processed and inverted using 1D Occam inversion (Constable et al., 1987).

Results and discussion

The synthetic modeling allowed us to determine suitable transmitter-receiver offsets and source frequencies for investigating OFG and SGD. Furthermore, to demonstrate and validate the functionality of the developed system, first results of the measured SWAN CSEM data collected during the Adriatic field test are presented.

Synthetic modeling results. By analyzing the spatial distribution of the in-line horizontal Ex and vertical Ez components of the electric field response to excitation of the 1D model depicted in Figure 4, we can ascertain the impact of sea and aquifer layers.

The Ex response shows its highest values in close proximity to the transmitter, which is positioned on the left edge of the figure at the air/sea interface. Conversely, the smallest values are observed in the deep seafloor at larger distances. The distortion of Ex caused by the presence of the resistive aquifer is clearly visible in Figure 4a. In contrast, the Ez response is notably reduced by the conductive seawater, while the aquifer, being more resistive (0.09 S/m) compared to the sediment overburden layer and basement layer (0.7 S/m), somewhat enhances it. Whether the Ez component is measurable close to the sea surface remains questionable due to its inherently small signal amplitude, corresponding signal-to-noise issues, and distortions caused by unsteady motion of the towed Ez receiver antenna (Goldman et al., 2015).

By studying the simulated electric field response as a function of distance from the transmitter on the sea surface, we observe that the Ex response of the model with the aquifer is larger than that of the no-aquifer model at ranges beyond 200 m (blue lines in Figure 5). On the other hand, the Ez response for the aquifer model is lower in amplitude than that of the no-aquifer model at offsets less than 500 m but higher at greater offsets (red lines in Figure 5). It is important to mention that, in this simulation, the in-line Ex response is the dominating component because its amplitude exceeds that of in-line Ez by almost three orders of magnitude. From a practical perspective, this information is relevant as Ex is easier to measure and less susceptible to signal-to-noise issues.

Systematically changing different model parameters in the canonical model illustrates that the seawater depth has a large effect on both Ex and Ez responses, generally causing amplitudes to decrease and lowering the aquifer response as the water depth increases from 10 to 200 m. This is the expected result for diffusive methods such as CSEM. Thus, a thorough modeling study should precede a field study to determine if the aquifer is detectable/resolvable at the anticipated water depth. Additionally, it is advisable to obtain a high-resolution bathymetry model to reduce uncertainties in the interpretation of the measured data. A comprehensive sensitivity analysis of the overburden layer thickness and resistivity was conducted by computing the absolute difference of the Ex response for models with and without the aquifer for 50, 200, and 350 m offsets and for three frequencies — 0.1, 1.0, and 10 Hz. The predominantly vertical orientation of the isolines in Figure 6 suggests that the Ex response to the aquifer is much more sensitive to overburden thickness than overburden conductivity. The largest effect is observed at the highest frequency (10 Hz) and the greatest offset (350 m) considered.

Starting from the analysis conducted using the 1D forward modeling, we considered transmitter-receiver offsets between 150 and 1000 m (see Figure 2). The sensitivity studies suggest that including receivers distributed from short to large offsets helps to constrain the shallow-sediment conductivity, which ultimately helps to resolve the aquifer in inversions of the data. The array was kept at 1 km in total length for logistical reasons.

Field test results. After collecting CSEM data in the central Adriatic, a preliminary quality control inspection assured that a good signal-to-noise ratio was obtained. When comparing the signal obtained from transmitting an electric current of 25 A (Figure 7c) to the signal measured without transmission (Figure 7d), it becomes evident that the amplitude of the signal measured with the active transmitter is approximately one to two orders of magnitude greater than the background noise. This significant difference allows for the analysis of the measured data without the need for extensive processing.

The power spectrum for both data sets acquired without transmitter current shows a pronounced peak in electromagnetic noise at about the 50 Hz frequency, which is attributed to electric power

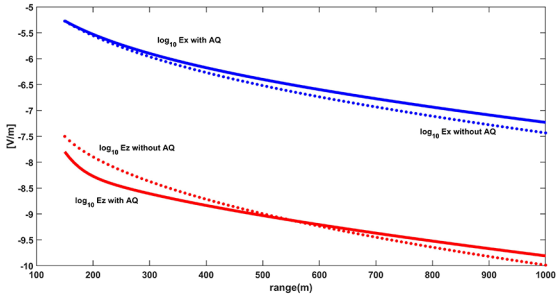

Figure 5. Response of the Ex (blue lines) and Ez (red lines) components of the electric field computed for a 1D model with aquifer (solid lines) and a 1D model without aquifer (dotted lines), detected at different distances from the transmitter, on the sea surface, and using a frequency source of 1 Hz.

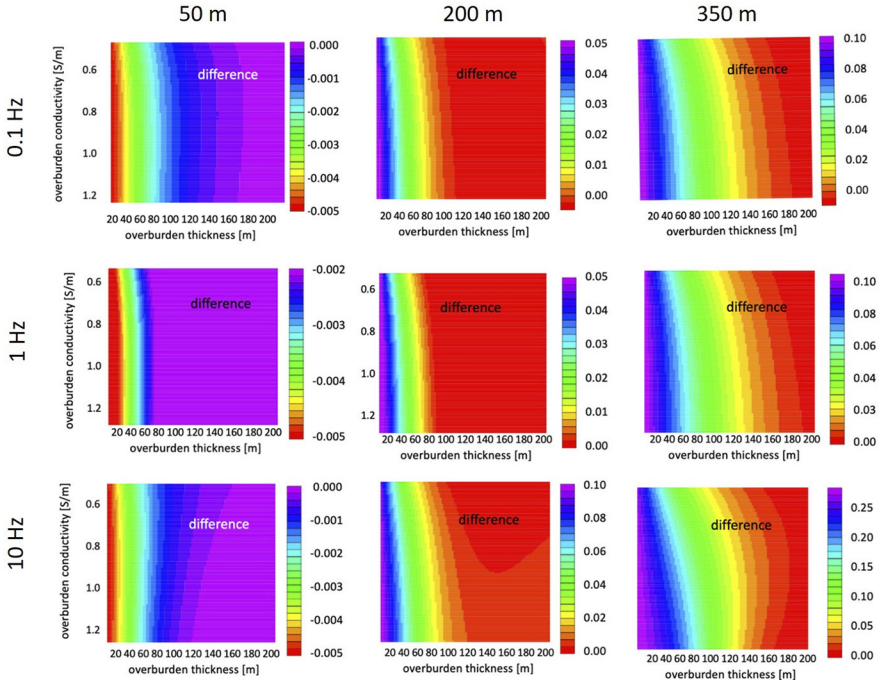

Figure 6. Absolute differences of Ex responses for the 1D model with aquifer and a 1D model without aquifer, computed considering different sediment overburden in terms of both thickness and resistivities, for a source frequency of 0.1 Hz (top row), 1 Hz (middle row), and 10 Hz (bottom row); and for 50 m range (left column); 200 m range (middle column); and 350 m range (right column).

DOI:10.1190/tle42090590.1

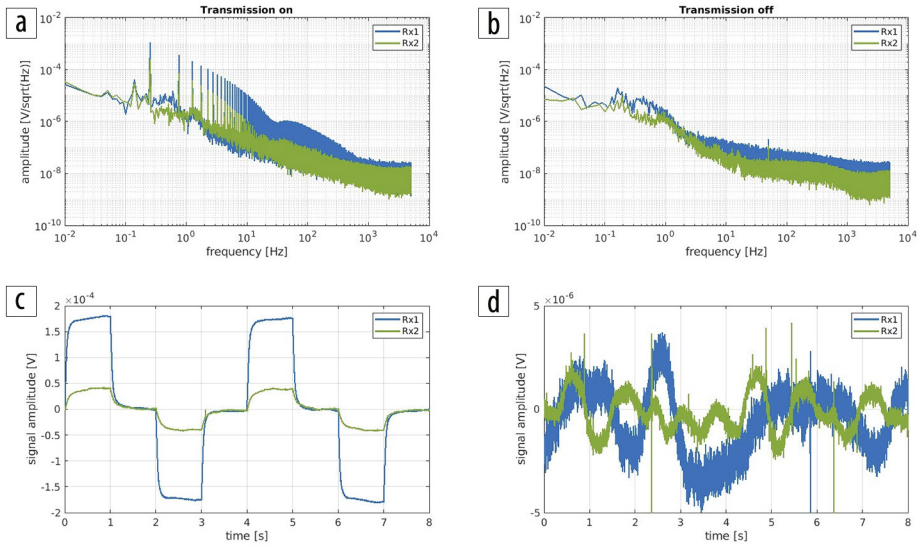

Figure 7. (a) Power spectra and (c) measured time series signals of the electrical field obtained by injecting 25 A current in the sea subsurface. (b) Power spectra and (d) measured time series background noise.

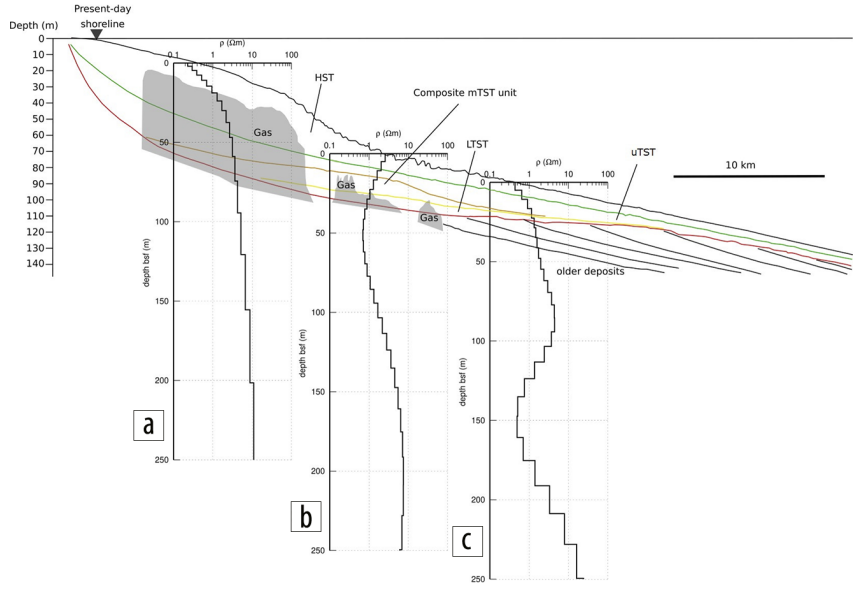

Figure 8. Overlay of resistivity-depth models using 1D Occam inversion and stratigraphic interpretations redrawn after Masselli et al. (2011). The seismic profile's location (ST05) on the map in Figure 3 is indicated. Resistivity depth model at (a) 15 m, (b) 60 m, and (c) 80 m water depth. The green, orange, and yellow lines indicate the interface boundaries between the highstand system tract (HST) and upper transgressive system tract (uTST), the uTST and middle transgressive system tract (mTST), and the mTST and low transgressive system tract (LTST). The red line denotes the modern depth of the unconformity associated with the latest sea-level fall. Presence of gas is determined through seismic blanking (see Masselli et al., 2011) and is denoted by gray areas. The depth of the resistivity model refers to depth below seafloor.

transmission lines and electronic devices of everyday use. Therefore, the high magnitude associated with this frequency in the Adriatic data set could be due to the proximity of the western Adriatic coast and possibly the extensive presence of offshore oil and gas platforms. When transmitting a current of 25 A (Figures 7a and 7c), these anthropogenic distortions are secondary compared to the excited source current. However, it should be noted that these noise considerations depend on the survey area and could play a more dominant role for measurements conducted closer to the coastline.

A data excerpt obtained along line 2 (cf. Figure 3) is processed and inverted to demonstrate the functionality of the system. This excerpt includes processed data acquired at approximately 15, 60, and 80 m water depths. Figure 8 shows the 1D inversion models, illustrated as resistivity-depth plots that overlay the stratigraphic interpretations obtained from seismic data of Maselli et al. (2011). At a shallow water depth close to the present-day shoreline, Maselli et al. (2011) indicate the presence of gas, resulting in a distinct increase of electrical resistivity from below 1 Ωm to approximately 6 Ωm with depth (left resistivity model). These values lie within the typical resistivity range for marine sediments and gas anomalies (e.g., Attias et al., 2018). The upper boundary and associated resistivity increase of the gas unit are well resolved by the CSEM data. The highstand deposits and transgressive system tract deposits appear as a conductor that overlay more resistive older deposits. At the profile center (water depth approximately 60 m), the bathymetry changes rapidly, and a 2D effect is expected to superimpose the acquired CSEM data. Here, the onset of an additional composite middle transgressive system tract deposit causes a thicker low-resistive unit to overlay the older deposits. The potential OFG body is expected within this depth range, but its presence cannot be confirmed using this preliminary 1D inversion approach. We note that the presented 1D resistivity model results are preliminary. The inversion intends only to demonstrate that the measured data can be fit with plausible resistivity values expected for marine environments. Here, the inversion models demonstrate that seawater-saturated sedimentary deposits will generally have resistivities of 0.5–2 Ωm. The presence of gas in the near-shore domain increases the resistivity with depth considerably, whereas CSEM data acquired at regions located farther from the shoreline agree with the stratigraphic interpretations of Maselli et al. (2011). However, a rigorous interpretation along each of the measured transects will require more extensive processing and 2D constraint/2D inversion and will thus follow at a later stage of the project.

Conclusions

The newly developed SWAN CSEM system reveals significant capability in mapping OFG and SGD, offering unique advantages in cost-effectiveness, modularity, and surface-towed capabilities that are suited for near-coastal operations in shallow

marine environments. Additionally, the system provides logistical benefits with its user-friendly design, allowing for efficient and independent operation without extensive technical assistance, thereby enhancing workflow efficiency, particularly for time-domain acquisition.

The field test data acquired by the system successfully demonstrates its functionality. By enabling continuous measurements in both time and frequency domains, the system is capable of acquiring high-quality data at speeds of 2.5–3 kn, effectively detecting resistivity variations in the subsurface up to depths of approximately 150–200 m. Higher penetration depths are feasible by increasing the transmitter-receiver offsets to more than 450 m.

One notable advantage of the SWAN system is its adaptability to different depths and varying resolution requirements. Its modular design allows for customization to suit various exploration needs, ensuring the acquisition of high-quality data even in complex geologic settings.

Despite the overall success of the test phase, certain challenges were encountered during measurements. The transmitter position system, designed for both land and sea operations, proved unsuitable for continuous measurements during vessel movement. The constant motion of the vessel caused periodic interruptions in the GPS-guided transmitter synchronization unit, requiring manual intervention to restart the transmission. To mitigate this issue, plans are underway to update the transmitter synchronization system, ensuring uninterrupted continuous measurements.

Overall, the SWAN system offers substantial advantages in addressing global research questions regarding OFG and SGD. Its cost-effectiveness, modularity, and surface-towed capabilities make it a valuable tool for studying these phenomena in near-coastal environments, providing insights into the complex dynamics of onshore–offshore fluid exchange. By overcoming logistical challenges and enhancing system capabilities, the system has the potential to contribute significantly to the advancement of understanding and managing OFG and SGD on a global scale. TLE

Acknowledgments

We wish to express our heartfelt appreciation to the reviewers, whose diligent work significantly contributed to improving the clarity and precision of our manuscript. Our sincere thanks go to the editors of *The Leading Edge* for their continuous support and encouragement throughout the publication process. We are grateful for the invaluable support provided by the Maltese Energy and Water R&I Grant Scheme 2021 (Energy and Water Agency). We would like to thank the staff from the G. Dallaporta, the National Research Council, Institute of Marine Science CNR-ISMAR, and the University of Bologna for their assistance during the field test. Special thanks are due to Katrin Schwalenberg and the Federal Institute for Geosciences and Natural Resources for lending a winch to conduct the measurements, as well as to B. Tezkan and the technicians at the University of Cologne for their unwavering technical support.

Data and materials availability

Data associated with this research are available and can be obtained by contacting the corresponding author.

Corresponding author: eliana.pastoressa@um.edu.mt

References

Amorosi, A., V. Maselli, and F. Trincardi, 2016, Onshore to offshore anatomy of a Late Quaternary source-to-sink system (Po Plain–Adriatic Sea, Italy): Earth-Science Reviews, **153**, 212–237, https://doi.org/10.1016/j.earscirev.2015.10.010.

Arévalo-Martínez, D. L., A. Haroon, H. W. Bange, E. Erkul, M. Jegen, N. Moosdorf, J. Schneider von Deimling, et al., 2023, Ideas and perspectives: Land–ocean connectivity through groundwater: Biogeosciences, **20**, no. 3, 647–662, https://doi.org/10.5194/bg-20-647-2023.

Asioli, A., F. Trincardi, J. J. Lowe, D. Ariztegui, L. Langone, and F. Oldfield, 2001, Submillennial scale climatic oscillations in the central Adriatic during the Lateglacial: Palaeoceanographic implications: Quaternary Science Reviews, **20**, no. 11, 1201–1221, https://doi.org/10.1016/S0277-3791(00)00147-5.

Attias, E., S. Constable, D. Sherman, K. Ismail, C. Shuler, and H. Dulai, 2021, Marine electromagnetic imaging and volumetric estimation of freshwater plumes offshore Hawai'i: Geophysical Research Letters, **48**, no. 7, https://doi.org/10.1029/2020GL091249.

Attias, E., D. Thomas, D. Sherman, K. Ismail, and S. Constable, 2020, Marine electrical imaging reveals novel freshwater transport mechanism in Hawai'i: Science Advances, **6**, no. 48, eabd4866, https://doi.org/10.1126/sciadv.abd4866.

Attias, E., K. Weitemeyer, S. Hölz, S. Naif, T. A. Minshull, A. I. Best, A. Haroon, M. Jegen-Kulcsar, and C. Berndt, 2018, High-resolution resistivity imaging of marine gas hydrate structures by combined inversion of CSEM towed and ocean-bottom receiver data: Geophysical Journal International, **214**, no. 3, 1701–1714, https://doi.org/10.1093/gji/ggy227.

Attias, E., K. Weitemeyer, T. A. Minshull, A. I. Best, M. Sinha, M. Jegen-Kulcsar, S. Hölz, and C. Berndt, 2016, Controlled-source electromagnetic and seismic delineation of subseafloor fluid flow structures in a gas hydrate province, offshore Norway: Geophysical Journal International, **206**, no. 2, 1093–1110, https://doi.org/10.1093/gji/ggw188.

Burnett, W. C., H. Bokuniewicz, M. Huettel, W. S. Moore, and M. Taniguchi, 2003, Groundwater and pore water inputs to the coastal zone: Biogeochemistry, **66**, 3–33, https://doi.org/10.1023/B:BIOG.0000006066.21240.53.

Cattaneo, A., and F. Trincardi, 1999, The late-Quaternary transgressive record in the Adriatic epicontinental sea: Basin widening and facies partitioning, *in* K. M. Bergman and J. W. Snedden, eds., Isolated shallow marine sand bodies: Sequence stratigraphic analysis and sedimentologic interpretation: SEPM, 127–146, https://doi.org/10.2110/pec.99.64.0127.

Chave, A. D., M. E. Everett, J. Mattsson, J. Boon, and J. Midgley, 2017, On the physics of frequency-domain controlled source electromagnetics in shallow water. 1: Isotropic conductivity: Geophysical Journal International, **208**, no. 2, 1026–1042, https://doi.org/10.1093/gji/ggw435.

Constable, S., P. K. Kannberg, and K. Weitemeyer, 2016, Vulcan: A deep-towed CSEM receiver: Geochemistry Geophysics Geosystems, **17**, no. 3, 1042–1064, https://doi.org/10.1002/2015GC006174.

Constable, S. C., R. L. Parker, and C. G. Constable, 1987, Occam's inversion: A practical algorithm for generating smooth models from electromagnetic sounding data: Geophysics, **52**, no. 3, 289–300, https://doi.org/10.1190/1.1442303.

Engelmark, F., J. Mattsson, A. McKay, and Z. Du, 2014, Towed streamer EM comes of age: First Break, **32**, no. 4, 75–78, https://doi.org/10.3997/1365-2397.32.4.74381.

Evans, R. L., and K. Key, 2016, Mapping offshore freshwater deposits using electromagnetic methods: Second Applied Shallow Marine Geophysics Conference, EAGE, https://doi.org/10.3997/2214-4609.201602169.

Everett, M. E., and A. D. Chave, 2019, Energy flow in terrestrial controlled-source electromagnetic geophysics: European Journal of Physics, **40**, no. 6, 065202, https://doi.org/10.1088/1361-6404/ab3de5.

Gehrmann, R. A., J. Dettmer, K. Schwalenberg, M. Engels, S. E. Dosso, and A. Özmaral, 2015, Trans-dimensional Bayesian inversion of controlled-source electromagnetic data in the German North Sea: Geophysical Prospecting, **63**, no. 6, 1314–1333, https://doi.org/10.1111/1365-2478.12308.

Goldman, M., V. Mogilatov, A. Haroon, E. Levi, and B. Tezkan, 2015, Signal detectability of marine electromagnetic methods in the exploration of resistive targets: Geophysical Prospecting, **63**, no. 1, 192–210, https://doi.org/10.1111/1365-2478.12151.

Gustafson, C., K. Key, and R. L. Evans, 2019, Aquifer systems extending far offshore on the U.S. Atlantic margin: Scientific Reports, **9**, no. 1, 8709, https://doi.org/10.1038/s41598-019-44611-7.

Haroon, A., K. Lippert, V. Mogilatov, and B. Tezkan, 2018, First application of the marine differential electric dipole for groundwater investigations: A case study from Bat Yam, Israel: Geophysics, **83**, no. 2, B59–B76, https://doi.org/10.1190/geo2017-0162.1.

Haroon, A., A. Micallef, M. Jegen, K. Schwalenberg, J. Karstens, C. Berndt, X. Garcia, et al., 2021, Electrical resistivity anomalies offshore a carbonate coastline: Evidence for freshened groundwater?: Geophysical Research Letters, **48**, no. 14, https://doi.org/10.1029/2020GL091909.

Jing, J.-E., Z.-L.Wu, M. Deng, Q.-X. Zhao, X.-H. Luo, G.-H. Tu, K. Chen, and M. Wang, 2016, Experiment of marine controlled-source electromagnetic detection in a gas hydrate prospective region of the South China Sea: Chinese Journal of Geophysics, **59**, no. 7, 2564–2572, https://doi.org/10.6038/cjg20160721.

King, R. B., W. R. Danskin, S. Constable, and J. M. Maloney, 2022, Identification of fresh submarine groundwater off the coast of San Diego, USA, using electromagnetic methods: Hydrogeology Journal, **30**, no. 3, 965–973, https://doi.org/10.1007/s10040-022-02463-y.

Levi, E., M. Goldman, G. Tibor, and B. Herut, 2018, Delineation of Subsea freshwater extension by marine geoelectromagnetic soundings (SE Mediterranean Sea): Water Resources Management, **32**, no. 11, 3765–3779, https://doi.org/10.1007/s11269-018-2018-1.

Lippert, K., and B. Tezkan, 2020, On the exploration of a marine aquifer offshore Israel by longoffset transient electromagnetics: Geophysical Prospecting, **68**, no. 3, 999–1015, https://doi.org/10.1111/1365-2478.12875.

Luijendijk, E., T. Gleeson, and N. Moosdorf, 2020, Fresh groundwater discharge insignificant for the world's oceans but important for coastal ecosystems: Nature Communications, **11**, no. 1, 1260, https://doi.org/10.1038/s41467-020-15064-8.

Maselli, V., E. W. Hutton, A. J. Kettner, J. P. Syvitski, and F. Trincardi, 2011, High-frequency sea level and sediment supply fluctuations during Termination I: An integrated sequence-stratigraphy and modeling approach from the Adriatic Sea (Central Mediterranean): Marine Geology, **287**, no. 1–4, 54–70, https://doi.org/10.1016/j.margeo.2011.06.012.

Micallef, A., M. Person, C. Berndt, C. Bertoni, D. Cohen, B. Dugan, R. Evans, et al., 2021, Offshore freshened groundwater in continental margins: Reviews of Geophysics, **59**, no. 1, e2020RG000706, https://doi.org/10.1029/2020RG000706.

Micallef, A., M. Person, A. Haroon, B. A. Weymer, M. Jegen, K. Schwalenberg, Z. Faghih, et al., 2020, 3D characterisation and quantification of an offshore freshened groundwater system in the Canterbury Bight: Nature Communications, **11**, no. 1, 1372, https://doi.org/10.1038/s41467-020-14770-7.

Pellegrini, C., A. Asioli, K. M. Bohacs, T. M. Drexler, H. R. Feldman, M. L. Sweet, V. Maselli, et al., 2018, The Late Pleistocene Po River lowstand wedge in the Adriatic Sea: Controls on architecture variability and sediment partitioning: Marine and Petroleum Geology, **96**, 16–50, https://doi.org/10.1016/j.marpetgeo.2018.03.002.

Schwalenberg, K., and M. Engels, 2011, Marine controlled source electromagnetic methods for gas hydrate assessment: New instrumentation and first results from the Black Sea test cruise: Schmucker-Weidelt-Kolloquium für Elektromagnetische Tiefenforschung, **24**, 239–249, https://gfzpublic.gfz-potsdam.de/pubman/item/item_65369, accessed 27 July 2023.

Sherman, D., P. Kannberg, and S. Constable, 2017, Surface towed electromagnetic system for mapping of subsea Arctic permafrost: Earth and Planetary Science Letters, **460**, 97–104, https://doi.org/10.1016/j.epsl.2016.12.002.

Spies, B. R., 1989, Depth of investigation in electromagnetic sounding methods: Geophysics, **54**, no. 7, 872–888, https://doi.org/10.1190/1.1442716.

Taniguchi, M., H. Dulai, K. M. Burnett, I. R. Santos, R. Sugimoto, T. Stieglitz, G. Kim, N. Moosdorf, and W. C. Burnett, 2019, Submarine groundwater discharge: updates on its measurement techniques, geophysical drivers, magnitudes, and effects: Frontiers in Environmental Science, **7**, 141, https://doi.org/10.3389/fenvs.2019.00141.

Tarquini, S., I. Isola, M. Favalli, A. Battistini, and G. Dotta, 2023, TINITALY, a digital elevation model of Italy with a 10 meters cell size (Version 1.1): Istituto Nazionale di Geofisica e Vulcanologia, https://doi.org/10.13127/tinitaly/1.1.

Wang, M., D. Ming, X. Li, Z. Zhang, H. Yue, T. Zhang, N. Duan, and X. Ma, 2021, The latest development of marine controllable source electromagnetic transmitter: IOP Conference Series: Earth and Environmental Science, **660**, 012137, https://doi.orghttps://doi.org/10.1088/1755-1315/660/1/012137.

Yuan, J., and R. N. Edwards, 2000, The assessment of marine gas hydrates through electrical remote sounding: Hydrate without a BSR?: Geophysical Research Letters, **27**, no. 16, 2397–2400, https://doi.org/10.1029/2000GL011585.